Condensed Matter Physics, 2002, Vol. 5, No. 2(30), pp. 285–305

CONDENSED MATTER PHYSICS

Star-polymer–colloid mixtures

J.Dzubiella, A.Jusufi

Institut für Theoretische Physik II, Heinrich-Heine-Universität Düsseldorf, Universitätsstraße 1, D-40225 Düsseldorf, Germany

Received October 9, 2001

Recent results in theory and simulation of star-polymer–colloid mixtures are reviewed. We present the effective interaction between hard, colloidal particles and star polymers in a good solvent derived by monomer-resolved Molecular Dynamics simulations and theoretical arguments. The relevant parameters are the size ratio q between the stars and the colloids, as well as the number of polymeric arms f (functionality) attached to the common center of the star. By covering a wide range of q's ranging from zero (star against a flat wall) up to about 0.5, we establish analytical forms for the star-colloid interaction which are in excellent agreement with simulation results. By employing this cross interaction and the effective interactions between stars and colloids themselves, a demixing transition in the fluid phase is observed and systematically investigated for different arm numbers and size ratios. The demixing binodals are compared with experimental observations and found to be consistent. Furthermore, we map the full two-component system on an effective one-component description for the colloids, by inverting the two-component Ornstein-Zernike equations. Some recent results for the depletion interaction and freezing transitions are shown.

Key words: *polymers, colloids, effective interaction, binary mixture, phase separation, depletion potential*

PACS: *82.70.Dd, 61.20.Gy, 64.70.-p*

1. Introduction

Typical soft matter systems, such as polymers and colloids, almost always occur in the form of mixtures. It is the central goal of soft matter physics to offer insights into the generic phase behaviour of such systems that does not depend on the detailed chemical structure of their constituents. In this respect, the study of mixtures of hard colloidal particles and non-adsorbing polymer *chains* has received a great deal of recent attention, both experimentally [1–3] and theoretically [3–6]. The theoretical approaches to the study of colloid-polymer mixtures were largely based on the Asakura-Oosawa (AO) model, in which the chains are envisaged as non-interacting spheres experiencing a hard-sphere repulsion with the colloids. This

model is most pertinent for Θ-like solvent conditions for the polymer. It can be mapped onto an effective one-component fluid featuring the so-called depletion interaction between the colloids, mediated by the ideal chains [3,4] and leading to fluid-fluid separation at polymer-colloid size ratios exceeding the value $q_c \cong 0.30$. Though the AO model provides an excellent benchmark for such systems, recent theoretical studies [5,6] and comparisons with experiments [2] indicate that the assumption of non-interacting chains leads to quantitative discrepancies between the two. Hence, a systematic effort to derive more realistic chain-chain [7] as well as chain-colloid [6,8] interactions has already been undertaken.

On the opposite end of the polymer-colloid mixture lies the binary hard sphere (BHS) mixture of large and small colloidal particles. Here, no fluid-fluid separation takes place [9]. It is therefore desirable to consider the systems that interpolate between the AO and the BHS models, in order to systematically investigate the evolution of the phase behaviour as we move from one extreme case to the other. Mixtures of colloids and nonadsorbing *star polymers* in a good solvent are such a natural bridge. A simple way to explore the thermodynamics of such mixtures is the use of pairwise interactions of the two mesoscopic components, having integrated out the monomer and solvent degrees of freedom. In binary mixtures three pair potentials are used as inputs for calculating structural quantities and phase behaviour with simulation or theory. In this work we give a review about the derivation of the star-colloid interaction and the main features of the phase behaviour of star-colloid mixtures.

The paper is organized as follows: in section 2.1 we present the general theoretical approach to the cross pair potential and derive analytic expressions for the star-wall interaction and for the star-colloid interaction for small size ratios. In section 2.2 we compare those with the results of monomer-resolved Molecular Dynamics simulations and determine the free parameters in order to achieve agreement between theory and simulation results. In section 3 we present the ensuing phase diagrams in the fluid phase by solving the full two-component system with fluid-integral equations. In section 4 we discuss some recent results for the depletion interaction and freezing transition of an effective one-component description of star-polymer–colloid mixtures. We conclude in section 5.

2. Interactions

2.1. Theory

Let us first define the system under consideration and its relevant parameters. We consider a collection of star polymers with functionality f and hard, spherical colloidal particles, the interaction between the latter species being modeled through the hard sphere (HS) potential:

$$V_{\mathrm{cc}}(r) = \begin{cases} \infty, & r \leqslant 2R_{\mathrm{c}} \\ 0, & \text{else.} \end{cases} \tag{1}$$

The colloids have a radius R_c, which is a well-defined length scale. The stars, on the other hand, are soft, hairy balls without a sharply defined boundary and this leads some freedom in defining length scales characterizing their spatial extent. The experimentally measurable length scale that naturally arises from small-angle neutron- or X-ray-scattering experiments (SANS or SAXS) is the radius of gyration R_g of the stars and the associated diameter of gyration $\sigma_g = 2R_g$. For the theoretical investigations on the subject, however, another length scale turns out to be more convenient, namely the so-called corona radius R_s of the star or the associated corona diameter $\sigma_s = 2R_s$. The corona radius arises naturally in the blob model for the conformation of isolated stars, introduced by Daoud and Cotton [10]. According to the Daoud-Cotton picture, the bulk of the interior of a star in good solvent conditions (and for sufficiently long arm chains), consists of a region in which the monomer density profile $c(s)$ follows a powerlaw as a function of the distance s from the star center, namely:

$$c(s) \propto a^{-3} \left(\frac{s}{a}\right)^{-4/3} \bar{v}^{-1/3} f^{2/3}, \tag{2}$$

with the monomer length a, the excluded volume parameter v and the reduced excluded volume parameter $\bar{v} \equiv v/a^3$. Outside this scaling region, there exists a diffuse layer of almost freely fluctuating rest chains, in which the scaling behaviour of the monomer profile is no longer valid. We define the corona radius R_s of the star as the distance from the center up to which the scaling behaviour of the monomer density given by equation (2) above holds true. In what follows, we define the *size ratio* q between the stars and the colloids as:

$$q \equiv \frac{R_g}{R_c}. \tag{3}$$

In addition, the interior of the star forms a semidilute polymer solution in which scaling theory [11] predicts that the osmotic pressure Π scales with the concentration c as $\Pi(c) \propto c^{9/4}$. Combining the latter with equation (2) above, we obtain for the radial dependence of the osmotic pressure of the star within the scaling regime the relation:

$$\Pi(s) \propto k_B T\, f^{3/2} s^{-3} \qquad (s \leqslant R_s). \tag{4}$$

In order to obtain a relation for the osmotic pressure $\Pi(s)$ for the diffuse region $s > R_s$ we examine the simplest case, in which a star center is brought within a distance z from a hard, flat wall, as depicted in figure 1.

Going back to an idea put forward some ten years ago by Pincus [12], we can calculate the force $F_{sw}(z)$ acting between the polymer and the wall by integrating the normal component of the osmotic pressure $\Pi(s)$ along the area of contact between the star and the wall. In the geometry shown in figure 1, this takes the form:

$$F_{sw}(z) = 2\pi \int_{y=0}^{y=\infty} \Pi(s) \cos\vartheta \, y \mathrm{d}y. \tag{5}$$

Using $z = s\,\cos\vartheta$ and $y = z\,\tan\vartheta$ we can transform equation (5) into:

$$F_{\rm sw}(z) = 2\pi z \int_z^\infty \Pi(s)\mathrm{d}s. \qquad (6)$$

Equation (6) above implies immediately that, if the functional form for the force $F_{\rm sw}(z)$ were to be known, then the corresponding functional form for the osmotic pressure $\Pi(z)$ could be obtained through:

$$\Pi(z) \propto -\frac{\mathrm{d}}{\mathrm{d}z}\left(\frac{F_{\rm sw}(z)}{z}\right). \qquad (7)$$

To this end, we now refer to the known, exact results regarding the force acting between a flat wall and a *single, ideal chain* one end of which is held at a distance z from a flat wall [13]. There, it has been established that the force $F_{\rm sw}^{\rm (id)}(z)$ is given by the relation:

$$F_{\rm sw}^{\rm (id)}(z) = k_{\rm B}T\frac{\partial}{\partial z}\ln\left[\mathrm{erf}\left(\frac{z}{L}\right)\right], \quad (8)$$

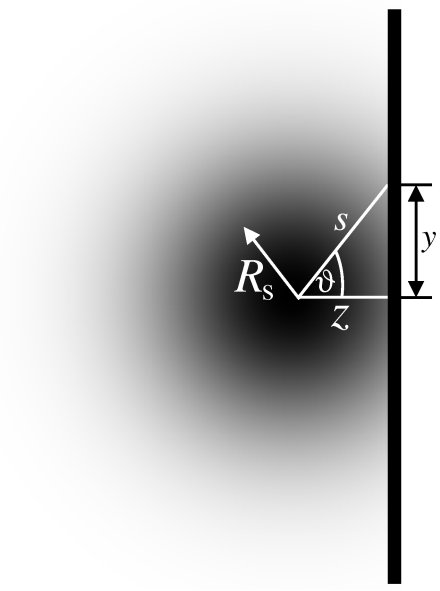

Figure 1. Star polymer (black-shadowed particle) interacting with a flat wall. The star polymer consists of an inner core region, where the scaling behaviour is dominant, whereas the outer regime is shadowed and indicates the exponential decay of the osmotic pressure.

where $\mathrm{erf}(x) = 2/\sqrt{\pi}\int_0^x \mathrm{e}^{-t^2}\mathrm{d}t$ denotes the error function and L is some length scale of the order of the radius of gyration of the polymer. Carrying out the derivative and setting $\mathrm{erf}\,(x) \cong 1$ or $x \gg 1$, we obtain a Gaussian form for the chain-wall force at large separations:

$$F_{\rm sw}^{\rm (id)}(z) \cong \frac{k_{\rm B}T}{L}\mathrm{e}^{-z^2/L^2} \qquad (z \gg L). \qquad (9)$$

We now imagine a star composed of ideal chains. As the latter do not interact with each other ("ghost chains"), the result of equation (9) holds for the star as well. Going now to self-avoiding chains, we assert that, as the main effect giving rise to the star-wall force is the volume which the wall excludes to the chains, rather than the excluded volume interactions between the chains themselves, a relation of the form (9) must also hold for the force $F_{\rm sw}(z)$ between a wall and a *real* star, but with the length scale L replaced by the radius of gyration or the corona radius of the latter and with an additional, f-dependent prefactor for taking into account the stretching effects of the f grafted polymeric chains. From equations (7) and (9) it now follows that

$$\Pi(s) \propto \frac{k_{\rm B}T}{L}\left(\frac{1}{s^2} + \frac{2}{L^2}\right)\mathrm{e}^{-s^2/L^2} \qquad (s \gg L). \qquad (10)$$

The full expression for $\Pi(s)$ now follows by combining equation (4), valid for $s \leqslant R_\mathrm{s}$, with equation (10), valid for $s \gg L \cong R_\mathrm{s}$, and matching them at $s = R_\mathrm{s}$. The local osmotic pressure $\Pi(s)$ in the interior of a star polymer, as a function of the distance s from its center has hence the functional form:

$$\Pi(s) = \Lambda f^{3/2} k_\mathrm{B}T \begin{cases} s^{-3} & \text{for } s \leqslant R_\mathrm{s} \\ \left(\frac{1}{s^2} + 2\kappa^2\right) \frac{\xi}{R_\mathrm{s}} \mathrm{e}^{-\kappa^2\left(s^2 - R_\mathrm{s}^2\right)} & \text{for } s > R_\mathrm{s}, \end{cases} \tag{11}$$

where Λ and $\kappa = L^{-1}$ are free parameters; it is to be expected that $\kappa = O(R_\mathrm{g}^{-1})$, as we will verify shortly. On the other hand, ξ must be chosen to guarantee that $\Pi(s)$ is continuous at $s = R_\mathrm{s}$, resulting in the value:

$$\xi = \frac{1}{1 + 2\kappa^2 R_\mathrm{s}^2}. \tag{12}$$

Equation (11) above concerns the radial distribution of the osmotic pressure of an isolated star. The question therefore arises, whether this functional form for the osmotic pressure can be used in order to calculate the force between a star and a flat wall also in situations where the star-wall separation is smaller than the radius of gyration of the star, in which case it is intuitively expected that the presence of the wall will seriously disturb the monomer distribution around the center and hence also the osmotic pressure. In fact, one intuitively expects that the osmotic pressure is a function of *both* the star-wall separation z and the radial distance s, whereas in what follows we are going to be using equation (6) together with equation (11), in which $\Pi(s)$ has no z-dependence. However, it turns out that this is an excellent approximation. On the one hand, it is physically plausible for large star-wall separations, where the presence of the wall has little effect on the segment density profile around the star center and the ensuing osmotic pressure profile. On the other hand, also at very small star-wall separations, the scaling form $\Pi(s) \propto s^{-3}$ continues to be valid. This claim can be corroborated by exact results for an ideal chain grafted on a hard wall [14], and scaling arguments [17]. One additional argument is the following:

Bringing a star with f arms at a small distance to a flat wall, creates a conformation which is very similar to the one of an isolated star with $2f$-arms, as shown in figure 2. Hence, it is not surprising that at small star-wall separations, one recovers for the radial dependence osmotic pressure the scaling laws pertinent to an isolated star. In addition, by inserting equation (11) into equation (6) and carrying out the integration, we find that for small star-wall distances, $z \ll R_\mathrm{s}$, the force scales as $F_\mathrm{sw}(z) \propto (k_\mathrm{B}T)/z$, thus giving rise to a logarithmic effective star-wall potential $V_\mathrm{sw}(z) \propto -k_\mathrm{B}T \ln(z/R_\mathrm{s})$. The latter is indeed in full agreement with predictions from scaling arguments arising in polymer theory [12,15,16]. This is an universal result, in the sense that it also holds for single chains, be they real or ideal. It can also be read off from the exact result, equation (8), using the property $\mathrm{erf}\,(x) \propto x$ for $x \to 0$. Thus, the proposed functional form for the osmotic pressure, equation (11), combined with equation (6) for the calculation of the effective force, has the following remarkable property: it yields the correct result both at small and at large

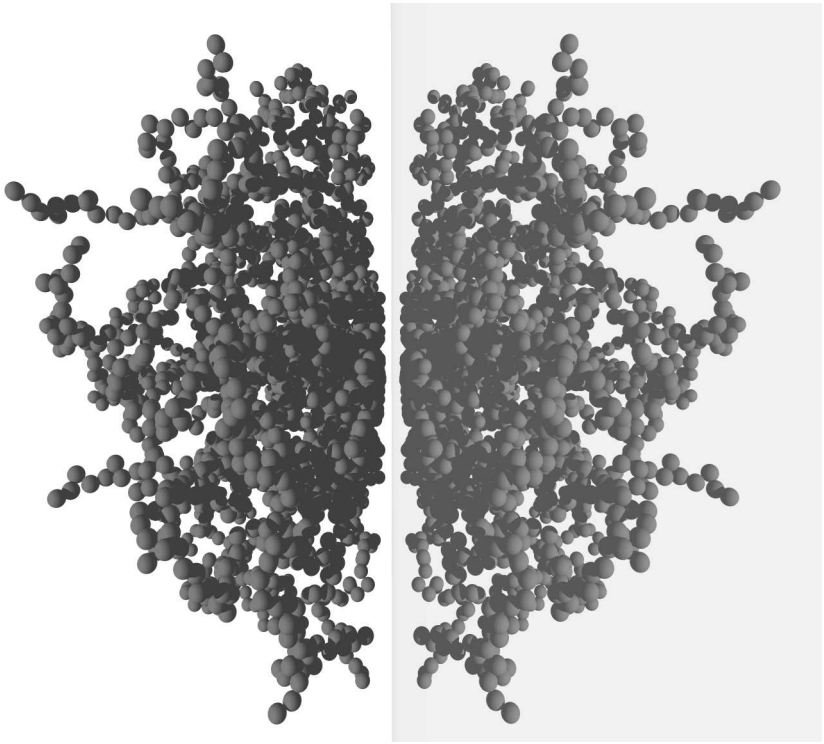

Figure 2. Snapshot of a simulation showing a star polymer interacting with a flat wall, at a small center-to-surface distance. The mirror-reflected image of the star, on the right, helps demonstrate that the configuration is similar to that of an isolated star with twice as many arms.

star-wall distances and therefore appears to be a reliable analytical tool for the calculation of the effective force at *all* star-wall distances. At the same time, it contains two free parameters, Λ and κ which allow some fine tuning when the predictions of the theory are to be compared with simulation results, as we will do below. Yet, we emphasize that this freedom is *not* unlimited: on physical grounds, κ must be of the order of $R_{\rm g}^{-1}$ and Λ must be a number of order unity for all functionalities f, as the dominant $f^{3/2}$-dependence of the osmotic pressure prefactor has already been explicitly taken into account in equation (11).

We are now in a position to write down the full expression for the star-wall force, by using equations (6) and (11). The result reads as:

$$\frac{R_{\rm s}F_{\rm sw}(z)}{k_{\rm B}T} = \Lambda f^{3/2}\begin{cases} \frac{R_{\rm s}}{z} + \frac{z}{R_{\rm s}}(2\xi - 1) & \text{for } z \leqslant R_{\rm s} \\ 2\xi \exp[-\kappa^2(z^2 - R_{\rm s}^2)] & \text{for } z > R_{\rm s}. \end{cases} \tag{13}$$

Note the dominant $\propto 1/z$-dependence for $z \to 0$. Accordingly, the effective interaction potential $V_{\rm sw}(z)$ between a star and a flat, hard wall held at a center-to-surface distance z from each other reads as:

$$\beta V_{\rm sw}(z) = \Lambda f^{3/2}\begin{cases} -\ln(\frac{z}{R_{\rm s}}) - (\frac{z^2}{R_{\rm s}^2} - 1)(\xi - \frac{1}{2}) + \zeta & \text{for } z \leqslant R_{\rm s} \\ \zeta\,\mathrm{erfc}(\kappa z)/\mathrm{erfc}(\kappa R_{\rm s}) & \text{for } z > R_{\rm s}, \end{cases} \tag{14}$$

with the inverse temperature $\beta = (k_\mathrm{B}T)^{-1}$, the additional constant

$$\zeta = \frac{\sqrt{\pi}\xi}{\kappa R_\mathrm{s}} \operatorname{erfc}(\kappa R_\mathrm{s})\, \mathrm{e}^{\kappa^2 R_\mathrm{s}^2} \tag{15}$$

and the complementary error function $\operatorname{erfc}(x) = 1 - \operatorname{erf}(x)$. This completes our theoretical analysis of the star polymer-wall force and the ensuing effective interaction potential. The comparison with simulation data and the determination of the free parameters in the theory will be discussed in section 2.2.

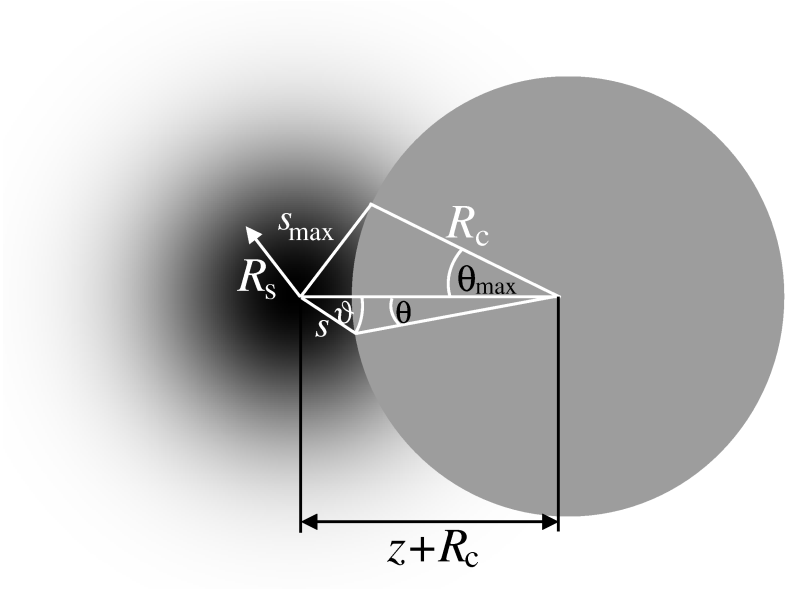

Figure 3. Star polymer (black-shadowed particle) interacting with a colloidal particle (grey sphere). The dark and shadowed regions of the star have the same meaning as in figure 1.

We now proceed with the calculation of the effective force between a star and a spherical hard particle, where effects of the colloid curvature become important. We apply the same idea as for the case of the hard wall: the effective force acting at the center of the objects is obtained by integrating the osmotic pressure exerted by the polymer on the surface of the colloid. In figure 3, the geometrical situation is displayed: within the corona radius of the star polymer $R_\mathrm{s} = \sigma_\mathrm{s}/2$, the osmotic pressure is determined by scaling laws; the outer regime is shadowed and signifies the Gaussian decay of the osmotic pressure. At center-to-surface distance z (center-to-center distance $r = z + R_\mathrm{c}$), the integration of the osmotic pressure is carried out over the contact surface between star and colloid. Taking into account the symmetry of the problem, e.g., its independence of the azimuthal angle, we obtain the force $F_\mathrm{sc}(z)$ between the star and the colloid as:

$$F_\mathrm{sc}(z) = 2\pi R_\mathrm{c}^2 \int_0^{\theta_\mathrm{max}} \mathrm{d}\theta\ \sin\theta\, \Pi(s) \cos\vartheta, \tag{16}$$

where ϑ and θ are polar angles emanating from the center of the star polymer and the colloid, respectively. The geometrical situation is shown in figure 3. The

maximum integration angle $\theta_{\max}$ is related to the maximum integration distance $s_{\max}$ [17]. By introducing equation (11) into equation (16), an analytical expression for the effective force can be calculated, see [17]. It should be noted that, as in the flat-wall case, the force scales as well as $F_{\rm sc}(z) \propto (k_{\rm B}T)/z$ for small distances.

Furthermore, in the case of small size ratios $q = R_{\rm g}/R_{\rm c}$, the interaction range is small compared to the colloid radius $R_{\rm c}$, and $s_{\max}$ can be set infinity. Then an analytical calculation of the effective star polymer-colloid potential $V_{\rm sc}^{\infty}(z)$ is possible and yields [17,18]:

$$\beta V_{\rm sc}^{\infty}(z) = \Lambda f^{3/2} \left(\frac{R_{\rm c}}{z + R_{\rm c}} \right) \times \begin{cases} -\ln(\frac{z}{R_{\rm s}}) - (\frac{z^2}{R_{\rm s}^2} - 1)(\xi - \frac{1}{2}) + \zeta & \text{for } z \leqslant R_{\rm s} \\ \zeta \, \mathrm{erfc}(\kappa z)/\mathrm{erfc}(\kappa R_{\rm s}) & \text{for } z > R_{\rm s} \end{cases} \quad (17)$$

with the constant ζ given by equation (15). Clearly, in the limit $R_{\rm c} \to \infty$ ($q \to 0$), corresponding to a flat wall, equation (17) reduces to the previously derived result, equation (14). It is a remarkable feature that all effects of curvature are taken into account by the simple geometrical prefactor $R_{\rm c}/(z + R_{\rm c})$, for sufficiently small size ratios q. In this respect, the above result bears close similarity to the well-known Derjaguin approximation [19].

Finally, we note that for the effective interaction between the stars applied in section 3 and 4 we take the expression proposed by Likos *et al.* [20] for arm numbers $f \gtrsim 10$, confirmed by computer simulations in [21]. The pair potential is modeled by an interaction which is also logarithmic for an inner core and shows a Yukawa-type exponential decay at larger distances [20,22]:

$$V_{\rm ss}(r) = \frac{5}{18} k_{\rm B}T f^{\frac{3}{2}} \begin{cases} -\ln(\frac{r}{\sigma_{\rm s}}) + \frac{1}{1+\sqrt{f}/2} & r \leqslant \sigma_{\rm s} \\ \frac{\sigma_{\rm s}/r}{1+\sqrt{f}/2} \exp(-\frac{\sqrt{f}}{2\sigma_{\rm s}}(r - \sigma_{\rm s})) & \text{else.} \end{cases} \quad (18)$$

For the case of small arm numbers $f \lesssim 10$, a slightly modified pair potential proposed in [21] is employed, where the Yukawa decay is replaced by a Gaussian decay:

$$V_{\rm ss}(r) = \frac{5}{18} k_{\rm B}T f^{\frac{3}{2}} \begin{cases} -\ln(\frac{r}{\sigma_{\rm s}}) + \frac{1}{2\tau^2\sigma_{\rm s}^2} & r \leqslant \sigma_{\rm s} \\ \frac{1}{2\tau^2\sigma_{\rm s}^2} \exp\left(-\tau^2(r^2 - \sigma_{\rm s}^2)\right) & \text{else,} \end{cases} \quad (19)$$

where $\tau(f)$ is a free parameter of the order of $1/R_{\rm g}$ and is obtained by fitting to computer simulation results, see [17,18]. More features of the pure one-component star polymer system are reviewed in this issue by C.N.Likos and H.M.Harreis.

2.2. Simulation

In order to check the theoretical prediction of the forces between stars and hard surfaces, we performed a monomer-resolved Molecular Dynamics (MD) simulation and calculated the mean force at the center of the star polymer to compare the data with theory. The model is based on the ideas of simulation methods applied to linear polymers and to a single star [23,24]. The main features are described in [17]. We have carried out simulations for a variety of arm numbers f and size ratios q, allowing

us to make systematic predictions for the f- and q-dependencies of all theoretical parameters. In attempting to compare the simulation results with the theoretical predictions, one last obstacle must be removed: in theory, the fundamental length scale characterizing the star is the corona radius R_s. The latter, however, is not directly measurable in a simulation in which, instead, we can only assess the radius of gyration R_g. However, we have previously found that the ratio between the two remains fixed for all considered arm numbers f, having the value $R_\mathrm{s}/R_\mathrm{g} \simeq 0.66$ [21]. We now proceed with the presentation of our MD results.

We consider at first a star polymer near a hard wall. The theoretical prediction of the effective interaction force is given in equation (13). First, we consider the limit of small separations, $z \to 0$, which allows us on the one hand to test the theoretical prediction $F_\mathrm{sw}(z) \cong k_\mathrm{B}T\Lambda f^{3/2}/z$ and on the other hand to fix the value of the prefactor Λ, which is expected to have in general a weak f-dependence. For this prefactor, some semi-quantitative theoretical predictions already exist [25,26]. Numerical values for the exponents are known from renormalization group theory and simulation [27,28] and yield $\Lambda(f = 1) \approx 0.83$ and $\Lambda(f = 2) \approx 0.60$. On the other hand, for very large functionalities, $f \gg 1$, one can make an analogy between a star at distance z from a wall and two star polymers the centers of which are kept at distance $r = 2z$ from each other [12]. Indeed, for very large f, the conformations assumed by two stars brought close to each other show that the chains of each star retract to the half-space where the center of the star lies, a situation very similar to the star-wall case, as can be seen in figure 2. Then, one can make the approximation $F_\mathrm{sw}(z) \cong F_\mathrm{ss}(2z)$, where F_ss denotes the star-star force. For the latter, it is known [20] that it has the form:

$$F_\mathrm{ss}(r) = \frac{5}{18} f^{3/2} \frac{1}{r} \qquad (r \to 0), \tag{20}$$

implying for the coefficient Λ the asymptotic behaviour:

$$\lim_{f\to\infty} \Lambda(f) \equiv \Lambda_\infty = \frac{5}{36} \cong 0.14. \tag{21}$$

Since there is no theory concerning the values of Λ in the intermediate regime of f, Λ is used as fit parameter. Its value can be obtained by comparing the force according to equation (17) to the simulation results. An accurate estimation can be found by plotting the inverse force versus small distances z, where the $1/z$-behaviour holds. The values for $\Lambda(f)$ can be immediately read off from the slope of the curves [17], and they are summarized in table 1. There we see that Λ is indeed a decreasing function of f but the asymptotic value $\Lambda_\infty = 5/36$ is still not achieved at arm numbers as high as $f = 100$. The decay parameter κ is fixed by looking at the force at larger separations and the obtained results are also summarized in table 1. As expected, κ is of the order R_g^{-1}. A monotonic increase of κ with the arm number f is observed, consistent with the view that for large f stars form compact objects with a decreasing diffuse layer beyond their coronae [20]. A comparison between simulation results and the star polymer-wall force for the whole range of the interaction using the fit parameters determined earlier are shown in figure 4.

Table 1. The fit parameters arising from the comparison between theory and simulation for the star-wall and star-colloid interaction. Λ is the overall prefactor and κ is the inverse Gaussian decay length, both used in equation (17). $\sigma_{\rm s} = 2R_{\rm s} = 0.66\,\sigma_{\rm g}$ denotes the corona diameter of the stars, as measured during the simulation.

f	Λ	$\kappa R_{\rm s}$
2	0.46	0.58
5	0.35	0.68
10	0.30	0.74
15	0.28	0.76
18	0.27	0.77
30	0.24	0.83
40	0.24	0.85
50	0.23	0.86
80	0.22	0.88
100	0.22	0.89

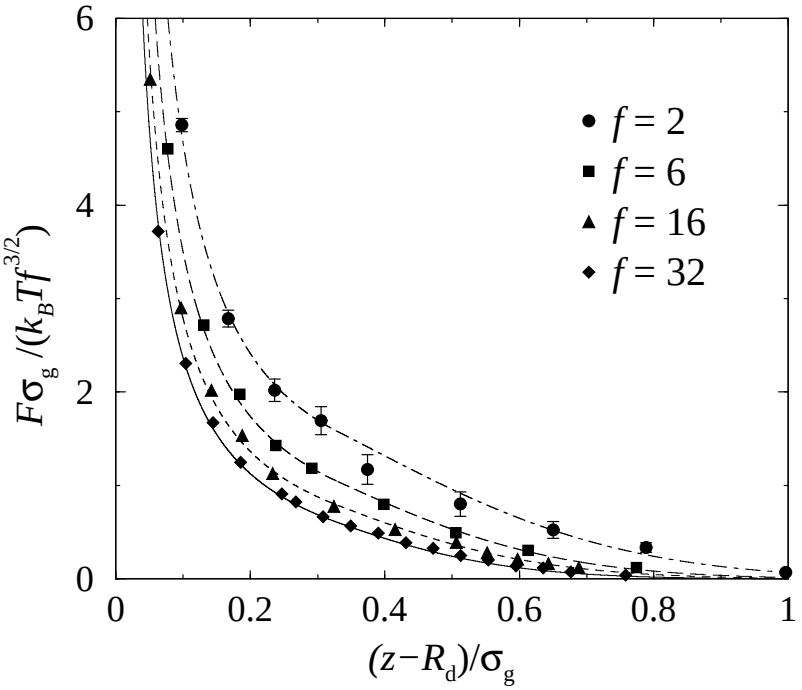

Figure 4. Effective force between a star polymer and a hard flat wall plotted against the distance z between the star center and the surface of the wall. Theoretical curves from equation (13) were compared to computer simulation data (symbols). For better comparison we divided the force by $f^{3/2}$. $R_{\rm d}$ is a small finite core size of the star in the simulation [17].

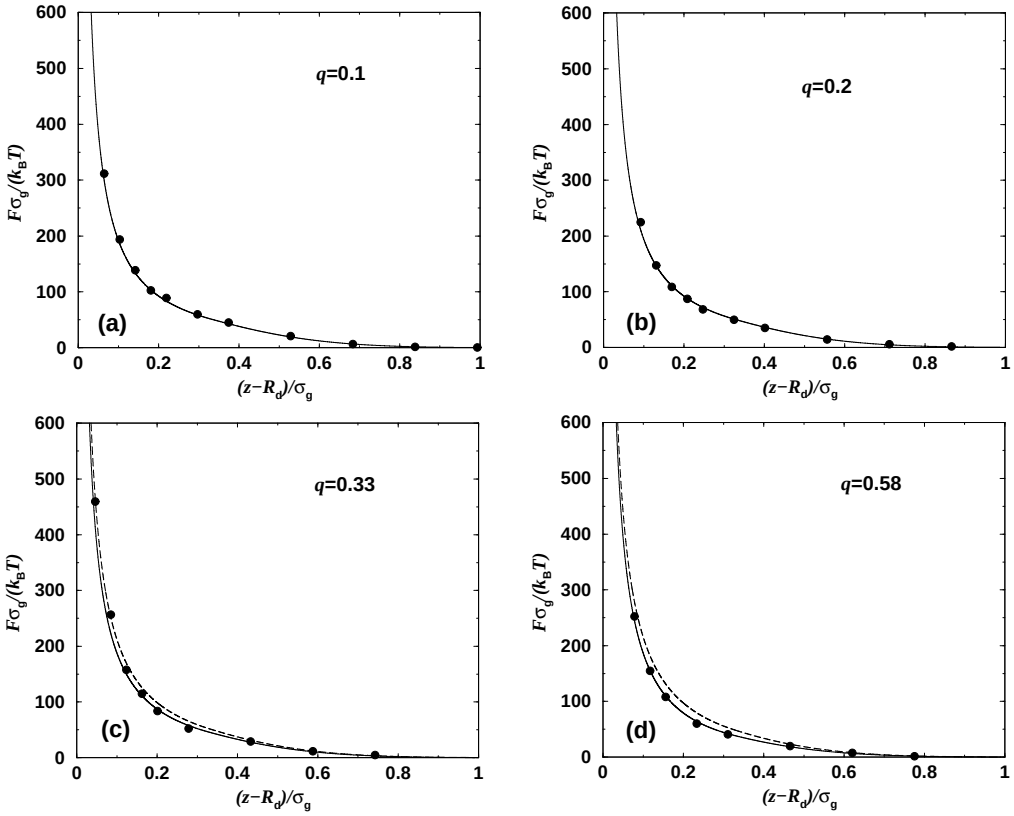

Figure 5. Comparison between simulation (symbols) and theoretical (lines) results for the effective force between a star polymer and a colloidal particle for different size ratios q, as a function of the center-to-surface separation z. The arm number here is $f = 18$. The solid lines in (a) and (b) show the force according to equation (17). In (c)-(d) the curves derived by means of this approximation are shown dashed and they increasingly deviate from the simulation results as q grows. Therefore, a finite upper integration limit has to be introduced (see the text), producing the curves denoted by the solid lines in (c)-(d) and bringing about excellent agreement with simulation. $R_{\rm d}$ is a small finite core size of the star in the simulation [17].

With parameters Λ and κ *once and for all fixed* from the star-wall case, we now turn our attention to the interaction of a star polymer at a hard sphere of finite radius $R_{\rm c}$, equivalently size ratios $q \neq 0$. Here, the force is given by the full expressions calculated in [17]. For small enough size ratios q, the approximation $\kappa s_{\rm max} \to \infty$ gives rise to a simplified expression for the force and to the analytical formula, equation (17) for the effective star-colloid potential. We show representative results for fixed arm number $f = 18$ and varying q in figure 5; results for different f-values are similar. It can be seen that the simplified result arising from allowing $s_{\rm max} \to \infty$ yields excellent results up to size ratios $q \lesssim 0.3$, see figures 5(a) and (b). However, above this value, the approximation of integrating the osmotic pressure up to infinitely large distances breaks down, as it produces effective forces that are larger than the simulation results, especially at distances z of the order of the ra-

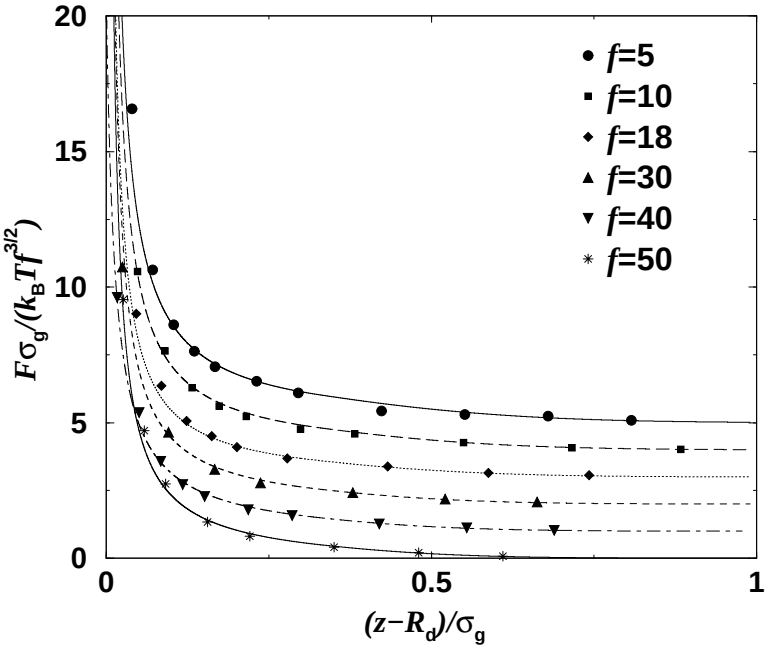

Figure 6. The effective force between a star polymer and a colloid for different arm numbers f and a size ratio $q = 0.33$ plotted against z, the distance of the star center to the surface of the colloid. The lines are the theoretical results while the symbols are the simulation ones. For clarity, the data have been shifted upwards by constants: $f = 10 : 1$, $f = 18 : 2$, $f = 30 : 3$, $f = 40 : 4$, $f = 50 : 5$. $R_{\rm d}$ is a small finite core size of the star in the simulation [17].

dius of gyration $R_{\rm g}$; these are the dashed lines shown in figures 5(c) and (d). The overestimation of the force is not surprising: as can be seen from figure 3 and equation (16), we are integrating a positive quantity beyond the physically allowed limits and this will inadvertently enhance the resulting force. Hence, we have to impose a finite upper limit $s_{\rm max}$ for size ratios $q > 0.3$ in order to truncate the contribution of the Gaussian tail in the integral of the osmotic pressure in equation (16).

We finally turn our attention to the f-dependence of the forces for a fixed value of the size ratio, $q = 0.33$. In figure 6 we show the simulation results compared with theory for a wide range of arm numbers, $5 \leqslant f \leqslant 50$. For the theoretical fits, the values of Λ and κ from table 1 were used, whereas the value of the maximum integration angle was kept fixed at $\theta_{\rm max} = 30^\circ$ for all f-values. The agreement between theory and simulation is very satisfactory.

3. Fluid phase behaviour

To access the fluid phase behaviour of the star polymer–colloid mixture on the level of effective pair potentials, we solve the Ornstein-Zernike equation for binary systems [29] closed with the Rogers-Young (RY) scheme [30]. Inputs are the pair potential for the colloids (1) and the analytical expression (17) for the star-colloid interaction. For the star polymers themselves, interactions (18) and (19) are applied.

The RY-closure is reliable for the one component star polymer system [31] and shows spinodal instability in highly asymmetric hard sphere mixtures [32]. Monte Carlo simulations using the above mentioned interactions and measuring the structure factors at selected thermodynamics points yield excellent agreement with RY. The thermodynamic consistency of the RY closure is enforced with a single adjustable parameter. Relevant thermodynamical parameters are the particle numbers N_c of the colloids and N_s of the stars leading to the total particle number $N = N_\mathrm{c} + N_\mathrm{s}$, and the packing fractions $\eta_\mathrm{c} = \frac{N_\mathrm{c}}{V}\frac{\pi}{6}\sigma_\mathrm{c}^3$ of the colloids and $\eta_\mathrm{s} = \frac{N_\mathrm{s}}{V}\frac{\pi}{6}\sigma_\mathrm{g}^3$ of the stars in the volume V.

The structure of binary mixtures is described by three partial static structure factors $S_{\alpha\beta}(k)$, with $\alpha, \beta = \mathrm{c}, \mathrm{s}$, obtained from RY. We find loci of points in the $(\eta_\mathrm{c}, \eta_\mathrm{s})$-plane at which the long wavelength limit $k \to 0$ of all structure factors diverges. This occurrence is an indication of a bulk instability and signals a demixing transition. The divergence of the structure factors is marking the *spinodal line* of the system. It is more convenient to consider the concentration structure factor $S_\mathrm{con}(k) = x_\mathrm{s}^2 S_\mathrm{cc}(k) + x_\mathrm{c}^2 S_\mathrm{ss}(k) - 2x_\mathrm{c}x_\mathrm{s}S_\mathrm{cs}(k)$, with the concentrations $x_\alpha = N_i/N$, $(\alpha = \mathrm{c}, \mathrm{s})$, which provides the approach to thermodynamics through [32,33]:

$$\lim_{k\to 0} S_\mathrm{con}(k) = k_\mathrm{B}T \left[\frac{\partial^2 g(x_\mathrm{c}, P, T)}{\partial x_\mathrm{c}^2}\right]^{-1}, \tag{22}$$

where $g(x_\mathrm{c}, P, T)$ is the Gibbs free energy $G(x_\mathrm{c}, N, P, T)$ per particle and P denotes the pressure of the mixture. If $g(x_\mathrm{c})$ has concave parts, the system phase-separates. The boundaries are calculated by the common tangent construction on the $g(x_\mathrm{c})$ vs. x_c curves at constant pressure. The results obtained are shown in figures 7 and 8.

Inside the spinodal line, the limits $S_{\alpha,\beta}(k \to 0)$ attain unphysical, negative values associated with the physical instability of the mixture against phase separation. Consequently, a solution of the integral equations is not possible there, and above the critical pressure P^*, $S_\mathrm{con}(x_\mathrm{c}, k = 0)$ is unknown in some interval $\Delta x_\mathrm{c}(P)$. Thus, it is necessary to interpolate $S_\mathrm{con}(x_\mathrm{c}, k = 0)$ in order to perform the integration of equation (22). In the vicinity of the critical point $\eta_\mathrm{c}^* \simeq 0.3$ the missing interval Δx_c is very small and the interpolation is reliable. Here the binodals should be accurate, while for higher pressures (packing fractions $\eta_\mathrm{c} < \eta_\mathrm{c}^*$ and $\eta_\mathrm{c} > \eta_\mathrm{c}^*$) the binodals are rather approximate but show reasonable behaviour. For highly asymmetric systems ($q \lesssim 0.18$) it becomes more and more difficult to get solutions of the integral equations in the vicinity of the spinodal line and the calculation of binodals is not possible.

The theoretical investigations were accompanied with experiments performed on commonly used star-polymer–colloid mixtures of varying composition [18]. The experimental samples were prepared by mixing polymethylmethacrylate (PMMA) suspensions and polybutadiene (PB) star polymer stock solutions. Each sample was homogenized by prolonged tumbling and allowed to equilibrate and observed by eye at room temperature $T = 25\,^\circ\mathrm{C}$. In all cases, demixing started within several hours, while crystallization started within two days. The comparison focuses only on the demixing transition.

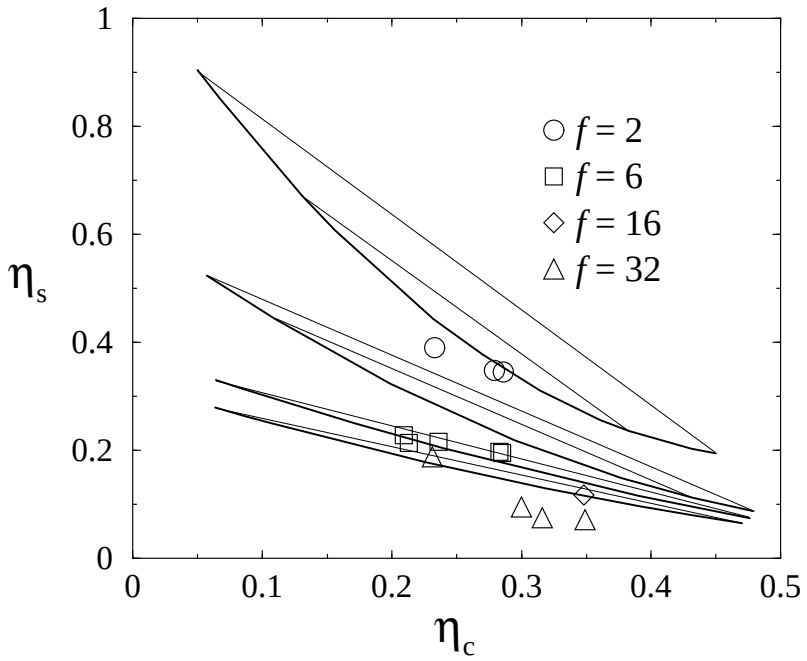

Figure 7. Binodals for the mixing-demixing transition in star polymer-colloid mixtures for different arm numbers $f = 2, 6, 16, 32$ (from top to bottom) and size ratio $q \approx 0.49$. Symbols mark experimental results compared with theory (lines) for $q = 0.50$. The thin straight lines are tielines connecting coexisting phases.

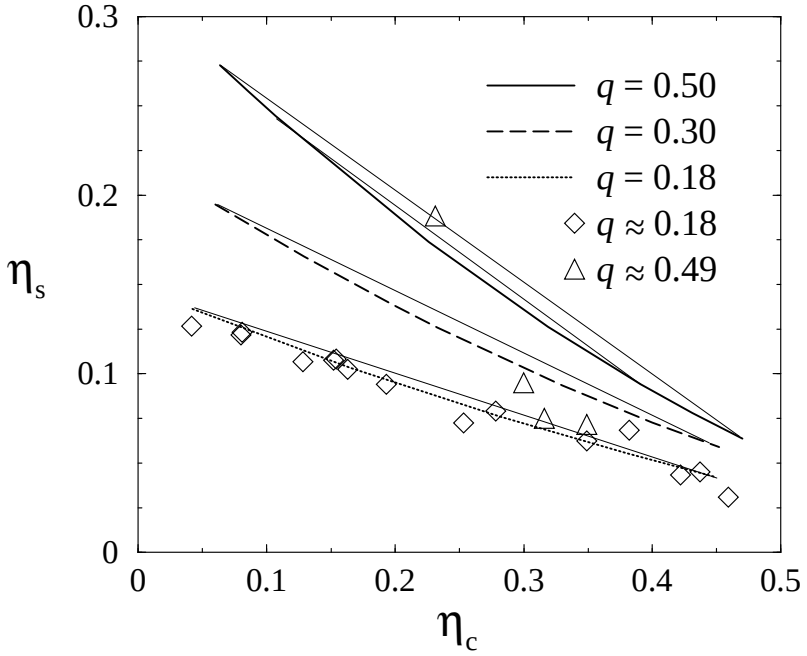

Figure 8. Same as in figure 7 for an arm number $f = 32$ and different size ratios q.

Comparison between theory and experimental are shown in figure 7 and 8. The good agreement is brought about *without* the use of any free parameters in the former that would allow for a rescaling of sizes or densities. In particular, the same trends are found as functions of the system parameters f and q. By increasing f at fixed q (figure 7), the demixing transition moves to lower star packing fractions η_s and the curves become flat. The most important observation from the results shown in figure 7 is that the $f = 2$ and $f = 32$ mixtures show qualitatively the same phase behaviour, namely a phase diagram with gas-liquid coexistence. From this point of view, a colloid + 32-arm star mixture still resembles a simple colloid polymer mixture rather than BHS. However, it is surprising that the phase boundary *drops* with increasing star functionality. Apparently, therefore, 32-arm stars are more efficient depletants than linear polymers.

When q is decreased but f remains fixed (figure 8), again a motion of the binodals to lower η_s is observed. This trend is *opposite* to the one predicted by the AO model (see figures 2(e)-(f) in [1].) The phase separation is not a simple hybrid between the AO and hard sphere mixtures but show a novel behaviour which one could trace back to non-additivity. A careful mapping of the current system into a nonadditive mixture would therefore be of interest. Yet, in view of the fact that the star-star and the cross interactions display soft tails, such a mapping is not straightforward and attempts in this direction are the subject of current investigations.

The absolute thermodynamic stability of the liquid phase will be influenced by the competing crystal phases that may preempt the demixing transition. Here, the exciting possibility opens up, that for size ratios $q \gtrsim 0.5$ and $f > 32$, colloid-star superlattices similar to those seen in the BHS may be stable, whereas for smaller size ratios and/or functionalities the crystals would be of the 'sublattice-melt' type. In this context, it may be significant that stars crystallize only when $f > 34$ [22]. However, for size ratios $q \lesssim 0.5$ and $f < 32$, which lies below the critical arm number $f_c = 34$ which is at least needed to freeze pure star solutions, it is to be expected that only the colloids will undergo crystallization. It is the competition between the demixing binodals against this freezing transition that we examine in the following section.

4. Effective one-component description

The calculation of the freezing transition for binary mixtures takes much computational effort. At the same time, theoretical approaches going beyond the binary hard sphere mixture are still lacking. To deal with this difficulty, a mapping onto an effective one-component system is useful. Here, a so-called depletion potential featuring attractive parts caused by the polymer component is acting between the colloids. The free energy can then be calculated by simple hard-sphere perturbation theory or thermodynamical integration. Effective one-component calculations were performed for the binary hard-sphere mixtures [4] and for the AO-potential [9], modelling colloid-polymer mixtures. Remarkably good agreement was found for the phase boundaries for all densities and size ratios comparing the one- and two-component descriptions.

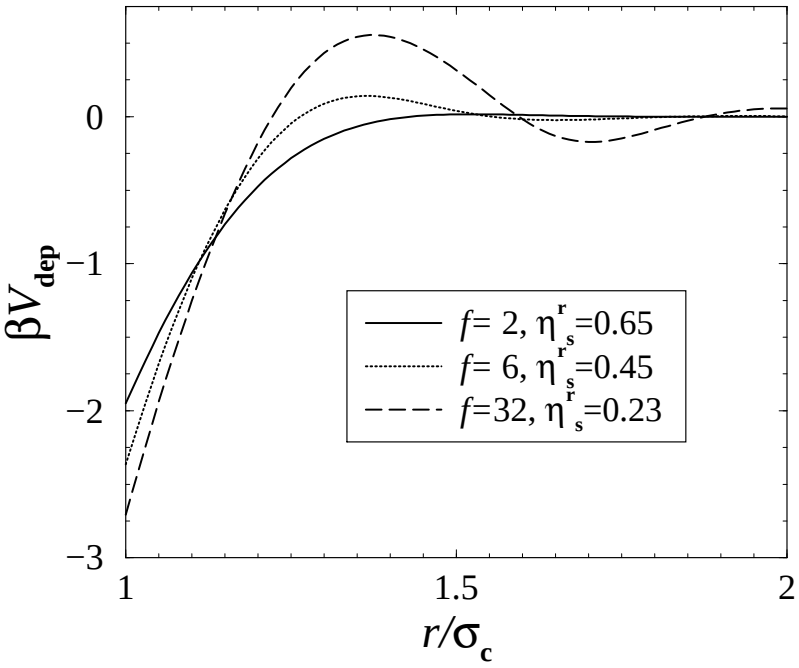

Figure 9. Depletion potentials $V_{\rm depl}$ for different arm numbers $f = 2, 6, 32$. The shown reservoir packing fractions $\eta_{\rm s}^{\rm r}$ are at the vicinity of the critical points of the gas-liquid transition, see figure 10. The size ratio is $q = 0.5$.

Neglecting higher body terms, one possible way to calculate the effective pair potential between the hard spheres is to solve the two-component OZ-equations in the low-density limit. Here the relation between pair correlation and pair potential is well known [29]:

$$\beta V_{\rm eff}(r) = -\lim_{\rho_{\rm c}\to 0} \ln[g_{\rm cc}(r;\rho_{\rm c})], \tag{23}$$

where the radial distribution function $g_{\rm cc}(r)$ of the colloids has evaluated at the low density limit. The effective potential depends additionally on the reservoir packing fraction $\eta_{\rm s}^{\rm r}$ describing the packing fraction of a reservoir of star polymers in contact with the colloids in low density limit. In [34] the effective force corresponding to (23) is compared to direct Monte-Carlo computer simulation results and excellent agreement is attained. The effective potential $V_{\rm eff}(r)$ splits up into the hard-sphere interaction (1) and the depletion potential $V_{\rm depl}(r)$:

$$V_{\rm eff}(r) = V_{\rm cc}(r) + V_{\rm depl}(r). \tag{24}$$

$V_{\rm depl}(r)$ is set to zero for distances $r < \sigma_{\rm c}$. Some examples of $V_{\rm depl}$ are shown in figure 9 for different arm numbers f and reservoir packing fractions $\eta_{\rm s}^{\rm r}$ near the critical point of the gas-liquid phase separation. The size ratio is $q = 0.5$. For distances $\sigma_{\rm c} \leqslant r \leqslant \sigma_{\rm c} + \sigma_{\rm g}$ depletion of the star polymers between the colloids gives rise to an effective attraction. While for $f = 2$ the interaction is purely attractive, the depletion interaction becomes oscillatory for increasing arm number. The oscillations are caused by increasingly strong star-star correlation effects as the star-star interaction becomes stiffer with increasing f, and are akin to those seen in BHS [4].

In order to determine the coexistence curves, the Helmholtz free energy $F = F(N_\mathrm{c}, V, \eta_\mathrm{s}^\mathrm{r})$ is needed. An accurate but computationally expensive way is to perform thermodynamical integration by MC simulation, using the hard-sphere system as reference. For a detailed description, see [4,9]. The free energy can be integrated by

$$F(N_\mathrm{c}, V, \eta_\mathrm{s}^\mathrm{r}) = F_0(N_\mathrm{c}, V, \eta_\mathrm{s}^\mathrm{r} = 0) + \int_0^1 \mathrm{d}\lambda \left\langle \sum_{i<j}^{N_\mathrm{s}} V_\mathrm{dep}(r) \right\rangle_{N_\mathrm{c}, V, \eta_\mathrm{s}^\mathrm{r}, \lambda}, \qquad (25)$$

while using an auxiliary effective interaction $V_\mathrm{eff}^\lambda(r)$ between the star-polymers and colloids in the simulation:

$$V_\mathrm{eff}^\lambda(r) = V_\mathrm{cc}(r) + \lambda V_\mathrm{dep}(r). \qquad (26)$$

Here, $0 \leqslant \lambda \leqslant 1$ is a dimensionless coupling parameter, allowing an interpolation between the hard sphere reference interaction ($\lambda = 0$) and the effective potential $V_\mathrm{eff}(r)$ ($\lambda = 1$) . For the free energy of the hard sphere reference system $F_0(N_\mathrm{c}, V, \eta_\mathrm{s}^\mathrm{r} = 0)$ we use the Carnahan-Starling expressions [35] for the fluid, and the equation of state proposed by Hall [36] for the solid phase. The calculation for every point of the free energy curve was performed with $N_\mathrm{s} = 108$ particles starting with a face-centered-cubic configuration. After fitting polynomials to $f = F/V$, the common tangent construction was employed to obtain the coexistence points. For more details we refer the reader to [9].

One can also obtain an upper bound for the sought-for free energy by employing a perturbation of the hard sphere interaction and then apply standard perturbation theory using the hard sphere system as reference system. In this approach the Helmholtz free energy of the perturbed system is obtained through the Gibbs-Bogolyubov inequality used as an equality and is given in first order by [29]

$$\frac{\beta F}{N} = \frac{\beta F_0}{N} + \frac{1}{2}\beta\rho \int \mathrm{d}^3 r \; g_0(r)\, V_\mathrm{dep}(r). \qquad (27)$$

Here, F_0 and $g_0(r)$ are the free energy and radial pair correlation function of the reference system and ρ is the number density. Barker and Henderson developed a second order term including two-body correlations [37], refining the free energy to

$$\frac{\beta F}{N} = \frac{\beta F_0}{N} + \frac{1}{2}\beta\rho \int \mathrm{d}\mathbf{r} \; g_0(r) V_\mathrm{dep}(r) - \left(\frac{\partial\rho}{\partial p}\right)_0 \frac{1}{4}\beta\rho \int \mathrm{d}\mathbf{r} \; g_0(r) V_\mathrm{dep}^2(r). \qquad (28)$$

In equation (28) above $(\partial\rho/\partial p)_0$ is the compressibility of the reference system. For the reference free energy F_0 we use the expressions of Carnahan-Starling and Hall, for the fluid and solid phases, respectively. The pair distribution functions $g_0(r)$ are provided by Verlet and Weis [38] for the fluid phase and by Kincaid and Weis [39] for the solid. Free energy calculations using equation (28) were performed by Dijkstra *et al.* for the effective Asakura-Oosawa pair potential, modelling colloid-polymer mixtures [4], and for the effective one-component binary hard sphere system [9].

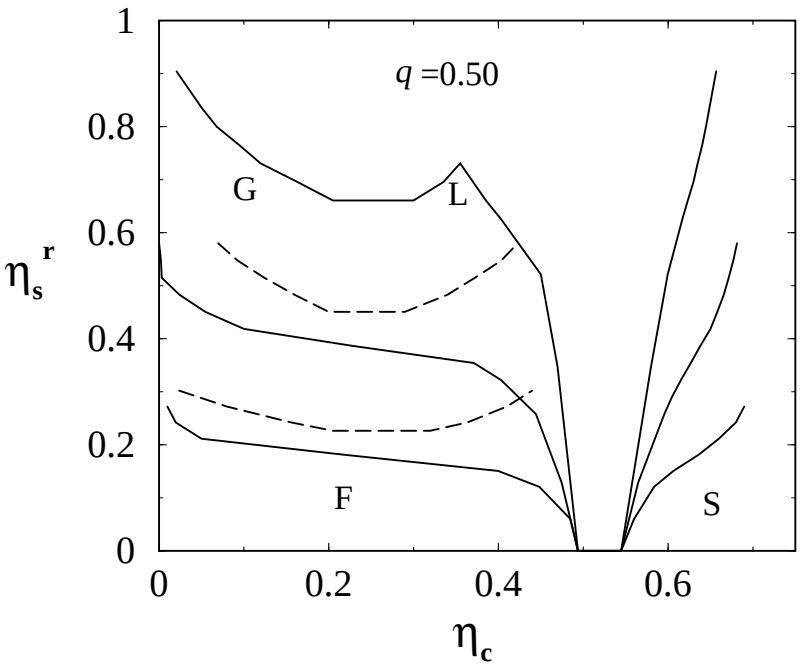

Figure 10. Phase diagram for a fixed size ratio $q = 0.5$ and different arm numbers $f = 2, 6, 32$ calculated with the effective one-component description. Reservoir packing fraction of the stars $\eta_{\rm s}^{\rm r}$ is plotted versus the colloid packing fraction $\eta_{\rm c}$. For $f = 2$ the system shows a stable gas (G) – liquid (L) transition, while for increasing arm number the gas-liquid transition becomes metastable (dashed lines) and decreases to lower reservoir densities $\eta_{\rm s}^{\rm r}$. The fluid (F) – solid (S) coexistence is broadening by increasing the arm number.

With this approach they found excellent agreement for the fluid-solid boundaries compared to thermodynamical integration results.

The comparison of the Helmholtz free energy calculated from the two different approaches described above, shows excellent agreement for the solid branch. For the fluid branch only the low density range of the perturbation approach coincides with the simulation results, whereas for larger densities the free energy is always too high. The reason is that the pair correlation function $g_{\rm cc}(r)$ of the colloids is extremely different compared to $g_0(r)$ of the reference hard sphere system in the fluid phase. Hence, for the calculation of the fluid phase behaviour the perturbation approach is not useful. We expect that a pure calculation with perturbation theory should give a good estimate of the freezing demixing transition, in agreement with Dijkstra *et al.* [4,9].

Therefore, the fluid branch is taken from thermodynamical integration and the solid branch from perturbation theory to reduce computational effort. Some resulting coexistence lines for fixed size ratio $q = 0.5$ and arm numbers $f = 2, 6, 32$ are plotted in figure 10. For the shown parameters only the $f = 2$ limit shows a stable gas-liquid coexistence. For increasing arm number, the demixing transition becomes metastable and occurs for lower reservoir packing fractions. Reaching the hard sphere limit $f \to \infty$ this transition should vanish. For every fixed size ratio q, a critical arm

number f^* should appear at which the stable gas-liquid transition occurs. We see that for our case $2 < f^* < 6$. The behaviour for different size ratios will be discussed in [40], where a comparison between the one- and two-component results will be presented as well.

5. Summary and concluding remarks

In conclusion we have presented analytical results for the force between a colloid and a star polymer in a good solvent, accompanied with an analytical expression for the corresponding pair potential which is valid for small size ratios. The validity of these expressions was established by direct comparison with Molecular Dynamics simulations. It should be noted that our theoretical approach is in principle generalizable to arbitrary geometrical shapes for the hard particle, thus opening up the possibility for studying effective forces between stars and hard ellipsoids, platelets etc. Using the derived interaction in fluid-integral equations we showed that the system demixes in the fluid phase and we calculated the demixing binodals for different arm numbers and size ratios. The binodals are in good agreement with experimental results. In order to determine the freezing transition, the full two-component system is mapped onto an effective one-component description by inversing fluid-integral equations in the low density limit. The results show that for a fixed size ratio a critical arm number occurs, at which the gas-liquid transition becomes metastable with respect to freezing.

One of the most useful features of star polymers is their hybrid character between polymers and colloids, through their tunable functionality f that allows a physical interpolation between chain behaviour ($f = 1, 2$) and colloid behaviour ($f \gg 1$). We have seen in this work how their hybrid character can be exploited for constructing depletants of variable quality in a HS system. The behaviour for different size ratios is investigated in [40]. Here, a critical size ratio appears at which the gas-liquid transition becomes metastable. Other interesting issues are a comparison with established models like the BHS mixture or the AO-model or a detailed study of the behavior of the depletion potential while changing the funcionality of the stars.

Acknowledgements

We thank C.N.Likos, C. von Ferber, H.Löwen, and J.Stellbrink for fruitful collaboration and A. Esztermann and C.N.Likos for a critical reading of the manuscript. This work has been supported by the Deutsche Forschungsgemeinschaft within the SFB 237.

References

1. Ilett S.M., Orrock A., Poon W.C.K., Pusey P.N. // Phys. Rev. E, 1995, vol. 51, p. 1344.
2. Moussaïd A., Poon W.C.K., Pusey P.N., Soliva M.F. // Phys. Rev. Lett., 1999, vol. 82, p. 225.

3. Lekkerkerker H.N.W., Poon W.C.K., Pusey P.N., Stroobants A., Warren P.B, // Europhys. Lett., 1992, vol. 20, p. 559.
4. Dijkstra M., Brader J.M., Evans R. // J. Phys.: Condens. Matter, 1999, vol. 11, p. 10079.
5. Louis A.A., Finken R., Hansen J.-P. // Europhys. Lett., 1999, vol. 46, p. 741.
6. Fuchs M., Shweizer K.S., // Europhys. Lett., 2000, vol. 51, p. 621.
7. Louis A.A., Bolhuis P.G., Hansen J.-P., Meier E.-J. // Phys. Rev. Lett., 2000, vol. 85, p. 2522.
8. Bolhuis P.G., Louis A.A., Hansen J.-P., Meier E.-J. // J. Chem. Phys., 2001, vol. 114, p. 4296.
9. Dijkstra M., van Roij R., Evans R. // Phys. Rev. E, 1999, vol. 59, p. 5744.
10. Daoud M., Cotton J.P. // J. Physique, 1982, vol. 43, p. 531.
11. Gennes P. G. Scaling Concepts in Polymer Physics. Ithaca, Cornell University Press, 1979.
12. Pincus P. // Macromolecules, 1991, vol. 24, p. 2912.
13. Eisenriegler E. Polymers Near Surfaces. Singapore, World Scientific, 1993.
14. Bickel T., Marques C.M., Jeppesen C. // Phys. Rev. E, 2000, vol. 62, p. 1124.
15. Witten T. A., Pincus P.A., Cates M.E. // Europhys. Lett., 1986, vol. 2, p. 137.
16. Witten T.A., Pincus P.A. // Macromolecules, 1986, vol. 19, p. 2509.
17. Jusufi A., Dzubiella J., Likos C.N., von Ferber C., Löwen H. // J. Phys.: Condens. Matter, 2001, vol. 13, p. 6177.
18. Dzubiella J., Jusufi A., Likos C.N., von Ferber C., Löwen H., Stellbrink J., Allgaier J., Richter D, Schofield A.B., Smith P.A., Poon W.C.K., Pusey P.N. // Phys. Rev. E, 2001, vol. 64, p. 010401(R).
19. Hunter R.J. Foundations of Colloid Science, vol. I. Oxford, Clarendon Press, 1986.
20. Likos C.N., Löwen H., Watzlawek M., Abbas B., Jucknischke O., Allgaier J., Richter D. // Phys. Rev. Lett., 1998, vol. 80, p. 4450.
21. Jusufi A., Watzlawek M., Löwen H. // Macromolecules, 1999, vol. 32, p. 4470.
22. Watzlawek M., Likos C.N., Löwen H. // Phys. Rev. Lett., 1999, vol. 82, p. 5289.
23. Grest G.S., Kremer K., Witten T.A. // Macromolecules, 1987, vol. 20, p. 1376.
24. Grest G.S. // Macromolecules, 1994, vol. 27, p. 3493.
25. Dietrich S., Diehl H.W. // Z. Phys. B, 1981, vol. 43, p. 315.
26. Ohno K., Binder K. // J. Phys. France, 1988, vol. 49, p. 1329.
27. Diehl H.W., Shpot M. // Nucl. Phys. B, 1998, vol. 528, p. 595.
28. Hegger R., Grassberger P. // J. Phys. A: Math. Gen., 1994, vol. 27, p. 4069.
29. Hansen J.-P., McDonald I.R. Theory of Simple Liquids. 2-nd ed. London, Academic Press, 1986.
30. Rogers F.A.,Young D.A. // Phys. Rev. A, 1984, vol. 30, p. 999.
31. Watzlawek M., Löwen H., Likos C.N. // J. Phys.: Condens. Matter, 1998, vol. 10, p. 8189.
32. Biben T., Hansen J.-P. // Phys. Rev. Lett., 1991, vol. 66, p. 2215.
33. Bhatia A.B., Thornton D.E. // Phys. Rev. B, 1970, vol. 2, p. 3004.
34. Dzubiella J., Likos C.N., Löwen H. // Europhys. Letters, 2002, vol. 58, p. 133.
35. Carnahan N.F., Starling K.E. // J. Chem. Phys., 1969, vol. 51, p. 635.
36. Hall K.R. // J. Chem. Phys., 1972, vol. 57, p. 2252.
37. Barker J.A., Henderson D.J. // J. Chem. Phys., 1967, vol. 47, p. 2856.
38. Verlet V.,Weis J.J. // Phys. Rev. A, 1972, vol. 5, p. 939.

39. Kincaid J.M., Weis J.J. // Mol. Phys., 1977, vol. 34, p. 931.
40. Dzubiella J., Likos C.N., Löwen H. // J. Chem. Phys, 2002, vol. 116, p. 9518.

Суміші зіркових полімерів і колоїдних частинок

Й.Дзубєлла, А.Юсуфі

Інститут теоретичної фізики II, Університет Гайнріха Гайне,
Університетштрассе 1, D-40225 Дюссельдорф, Німеччина

Отримано 9 жовтня 2001 р.

Зроблено огляд недавніх робіт про теорію та чисельне моделювання сумішей зіркових полімерів і колоїдних частинок. Приведено потенціал ефективної взаємодії між твердими колоїдними частинками і зірковими полімерами в доброму розчиннику, отриманий з комп'ютерного моделювання мономерів методами молекулярної динаміки та з теоретичних аргументів. Суттєвими параметрами потенціалу є співвідношення розмірів зірок і колоїдів q, а також кількість полімерних гілок (функціональність) f, приєднаних до спільного центра зірки. Знайдено аналітичну форму потенціалу взаємодії зірка-колоїд у широкій ділянці зміни q від нуля (зірка навпроти плоскої стінки) до величини порядку 0.5. Знайдена функція чудово узгоджується з результатами комп'ютерного моделювання. Використовуючи цей потенціал взаємодії, а також потеціали взаємодії між самими зірками і колоїдами, спостережено перехід розшарування в плинній фазі і проведено його систематичне дослідження для різної кількості ланцюгів і співвідношення розмірів. Бінодалі розшарування порівняно з експериментальними спостереженнями і виявлено взаємне узгодження. Більше того, ми зображуємо повну двокомпонентну систему як ефективну однокомпонентну для колоїдів, перетворюючи двокомпонентні рівняння Орнштайна-Церніке. Показано деякі недавні результати для взаємодії збіднення (depletion interaction) і фазових переходів в заморожений стан.

Ключові слова: *полімери, колоїди, ефективна взаємодія, бінарна суміш, фазове розділення, потенціал збіднення*

PACS: *82.70.Dd, 61.20.Gy, 64.70.-p*